Research Article GU J Sci 38(3): 1262-1274 (2025) DOI: 10.35378/gujs.1677631

Gazi University

Journal of Science

http://dergipark.org.tr/gujs

Attitude Control of Fixed-Wing UAVs under Input Constraints

Alper BAYRAK*

Bolu Abant İzzet Baysal University, Electrical and Electronics Engineering, 14030, Bolu, Türkiye

Highlights

- Control scheme for attitude control of fixed-wing UAVs under input saturation is investigated.
- A high-gain backstepping controller is designed using Lyapunov-based methods.
- A neural network is employed to compensate for the effects of control signal saturation.

Article Info

Received: 16 Apr 2025
Accepted: 21 June 2025

Keywords

Fixed-wing UAV, Backstepping control, Input saturation, Lyapunov stability analysis

Abstract

Fixed-wing unmanned aerial vehicles (UAVs) have gained widespread use in both civilian and military applications due to their low cost, long endurance, and high operational efficiency. However, ensuring precise attitude control under physical constraints such as input saturation remains a significant challenge. This study addresses the attitude control problem of fixed-wing UAVs under input constraints. The system model is divided into two subsystems, and a high-gain backstepping controller is designed. A neural network term is incorporated into the control method to overcome the effects of the residual control signal. The performance of the proposed control scheme is demonstrated through numerical simulations, showing that the method operates efficiently even in the presence of noise in the state variables.

1. INTRODUCTION

Fixed-wing unmanned aerial vehicles (UAVs) have become indispensable tools in both military and civilian domains today. This is because they offer low production and maintenance costs, high endurance, long flight hours, and high speeds. Thanks to these features, they are employed for various purposes such as surveillance, mapping, target tracking, and military applications. These vehicles are expected to operate under all weather conditions and across a wide range of altitudes. At this point, the precision attitude control of UAVs becomes a critical concern. The literature includes numerous studies on the control of fixed-wing UAVs, and some of these studies are summarized below.

Kimathi and Lantos presented a cascade control architecture which uses nonlinear inversion and PI controller for tracking of attitude angles [1]. Melkou *et al.* used super-twisting sliding mode controller for altitude control of fixed-wing UAV [2]. Bao *et al.* utilized adaptive sliding mode control in a backstepping design for attitude and altitude control [3]. In [4], Bohn *et al.* proposed a deep reinforcement learning controller for attitude control of fixed-wing UAV. Chen *et al.* handled the attitude tracking control problem for the cruise mode of an UAV in the presence of parameter uncertainties, unmodeled uncertainties and wind disturbances. They first designed a fixed-time observer to estimate the lumped disturbance then utilized sliding mode method for attitude control [5]. Poksawat *et al.* developed an automatic tuning algorithm for PID control of a fixed-wing UAV [6]. SaiCharanSagar *et al.* presented a backstepping algorithm combined with a inertial delay controller to handle time varying uncertainties and disturbances [7]. Ulus and Eski investigated the performances of the controller methods such as classical PID, artificial neuro-fuzzy inference system, fuzzy logic, combined ANFIS-PID, and PD-Fuzzy-PI for the control of fixed-wing UAV [8].

*e-mail: alperbayrak@ibu.edu.tr

The attitude of a UAV is controlled using control surfaces such as the aileron, elevator, and rudder. The deflections of these control surfaces are limited by their physical constraints, commonly referred to as input saturation. Input saturation can negatively affect system behavior and may even lead to instability. In the literature, several studies address input saturation in the control of fixed-wing UAVs. Zhao *et al.* considered the spatio-temporal trajectory tracking problem and proposed an exponential predefined-time controller to ensure that the fixed-wing UAV, under saturated input conditions, tracks the desired trajectory within a finite time [9]. Yu *et al.* developed a finite-time fault-tolerant control approach for fixed-wing UAVs, addressing actuator failures and input saturation to ensure attitude tracking [10]. Li *et al.* developed an adaptive fault-tolerant attitude tracking controller based on reinforcement learning for flying-wing UHV subjected to actuator faults and saturation [11]. Oh *et al.* presented a framework to guarantee the stability for a class of second-order nonlinear systems under multiple state and input constraints and applied the method to a fixed-wing UAV [12]. Wu *et al.* developed an adaptive sliding mode fault-tolerant control strategy, incorporating an adaptive auxiliary controller to handle input saturation and ensure fault-tolerant path-following performance [13].

This study focuses on the attitude control of UAVs under input constraints. The aim of the study is to present a control scheme that ensures the stability of tracking performance despite saturated inputs. A high-gain control method was designed for attitude control. Subsequently, a neural network term was incorporated into the control scheme to address the residual part of the control signal. The proposed scheme is inspired by the study in [14] and is implemented within a backstepping scheme. Unlike existing approaches in the literature on fixed-wing UAVs, it offers a framework that facilitates the application of various control methodologies. The neural network term is employed to ensure the boundedness of the error system, irrespective of the selected control method. The stability analysis was performed using a Lyapunov-based method, ensuring the ultimate boundedness of error signals. The effectiveness of the proposed control scheme was tested through numerical simulations. Simulation studies demonstrated the success of the method even in the presence of noise.

The rest of the paper is organized as follows: In section 2, the system model is presented. Control design and stability analysis are given in section 2 and 4, respectively. Finally, concluding remarks are presented in section 6.

2. SYSTEM MODEL

The rotational dynamics for the fixed-wing UAV can be represented by the equations below [15]:

$$\dot{\Omega} = R\omega, \tag{1}$$

$$\dot{\omega} = F(\omega) + \Psi\delta \tag{2}$$

where $\Omega = [\phi, \theta, \psi]^T$ is the attitude angle vector, $\omega = [p, q, r]^T$ is the angular rate vector, $\delta = [\delta_a, \delta_e, \delta_r]^T$ is control input vector, and $F(\omega) = [F_1, F_2, F_3]^T$ defining as

$$F_1 = \Gamma_1 pq - \Gamma_2 qr + \frac{1}{2}\rho V_a^2 Sb\left[C_{p_o} + C_{p_\beta}\beta + C_{p_p}\frac{bp}{2V_a} + C_{p_r}\frac{br}{2V_a}\right], \tag{3}$$

$$F_2 = \Gamma_5 pr - \Gamma_6(p^2 - r^2) + \frac{\rho V_a^2 SC}{2I_y}\left[C_{m_o} + C_{m_\alpha}\alpha + C_{m_q}\frac{Cq}{2V_a}\right], \tag{4}$$

$$F_3 = \Gamma_7 pq - \Gamma_1 qr + \frac{1}{2}\rho V_a^2 Sb\left[C_{r_o} + C_{r_\beta}\beta + C_{r_p}\frac{bp}{2V_a} + C_{r_r}\frac{br}{2V_a}\right] \tag{5}$$

where $\Gamma_1 = (I_{xz}(I_x - I_y + I_z))/\Gamma$, $\Gamma_2 = (I_z(I_z - I_y) + I_{xz}^2)/\Gamma$, $\Gamma_3 = (I_z)/\Gamma$, $\Gamma_4 = (I_{xz})/\Gamma$, $\Gamma_5 = (I_z - I_x)/I_y$, $\Gamma_6 = (I_{xz})/I_y$, $\Gamma_7 = ((I_x - I_y)I_x + I_{xz}^2)/\Gamma$, $\Gamma_8 = I_x/\Gamma$ and $\Gamma = I_x I_z - I_{xz}^2$.

The matrix Ψ is given as

$$\Psi = \begin{bmatrix} \frac{1}{2}\rho V_a^2 SbC_{p_{\delta_a}} & 0 & \frac{1}{2}\rho V_a^2 SbC_{p_{\delta_r}} \\ 0 & \frac{\rho V_a^2 SC}{2I_y} C_{m_{\delta_e}} & 0 \\ \frac{1}{2}\rho V_a^2 SbC_{r_{\delta_a}} & 0 & \frac{1}{2}\rho V_a^2 SbC_{r_{\delta_r}} \end{bmatrix} \tag{6}$$

and the transition matrix R is

$$R = \begin{bmatrix} 1 & \sin(\phi)\tan(\theta) & \cos(\phi)\tan(\theta) \\ 0 & \cos(\phi) & -\sin(\phi) \\ 0 & \sin(\phi)/\cos(\theta) & \cos(\phi)/\cos(\theta) \end{bmatrix}. \tag{7}$$

The parameters are defined in Table 1. For more detailed definitions, the reader is referred to [15].

Table 1. *Definitions of parameters*

Parameter	**Definition**
ϕ, θ, Ψ	roll, pitch and yaw angles
p, q, r	roll, pitch, yaw angular rates
α, β	angle of attack and side-slip angles
$\delta_a, \delta_e, \delta_r$	aileron, elevator and rudder deflections
V_a	airspeed of UAV
ρ	density of air
b, S, C	wing span, wing area, average cord length
J_{ab}	initial moments about *a* and *b* axes
C_*	aerodynamic coefficients
$I_{x,y,z}$	Moment of inertia about *x, y, z* axes
I_{xz}	Product moment of inertia

3. CONTROL DESIGN

The control objective is to ensure the Ω tracks the desired trajectory Ω_d, while keeping system states bounded, under input constraints.

Prior to the control design process, the system model in (2) is reformulated as:

$$\dot{\omega} = F(\omega) + \Psi\delta_s \tag{8}$$

where δ_s represents the saturated control input, expressed as:

$$\delta_{si} = \begin{cases} \delta_{min}, & \delta_i \leq \delta_{min} \\ \delta, & \delta_{min} \leq \delta_i \leq \delta_{max}, \\ \delta_{max}, & \delta_i \geq \delta_{max} \end{cases} \tag{9}$$

with δ_{min} and δ_{max} denoting the lower and upper bounds of the control input, respectively, δ_{si} and δ_i denoting the ith element of δ_s and δ, respectively. The saturated signal can also be expressed as:

$$\delta_s \triangleq \delta + \beta \tag{10}$$

where β accounts for the residual portion of the control input. This residual can be modeled using a neural network structure as:

$$\beta = W^T \sigma(X) + \varepsilon \tag{11}$$

where $W \in \mathbb{R}^{12\times 3}$ is the constant weight matrix, $\sigma(\cdot): \mathbb{R}^{12} \to \mathbb{R}^{12}$ is the activation function, $\varepsilon(t) \in \mathbb{R}^3$ is the functional approximation error, and $X(t) \in \mathbb{R}^{12}$ is a vector consisting of state variables related to the control input.

The following assumptions are made throughout the control design process:

Assumption 1 The system states Ω and ω are fully available.

Assumption 2 The reference trajectory Ω_d and its derivatives up to the second order are bounded.

The control design process starts by defining the objective error $e(t) \in \mathbb{R}^3$ and the system error $z(t) \in \mathbb{R}^3$ as follows

$$e \triangleq \Omega - \Omega_d, \tag{12}$$

$$z \triangleq \omega - \omega_d \tag{13}$$

where $\omega_d(t)$ represents the desired angular velocity and serves as the virtual control input for the backstepping approach. By differentiating (12) with respect to time,

$$\dot{e} = R\omega_d + Rz - \dot{\Omega}_d \tag{14}$$

is obtained, where (1) and (13) are used.

The virtual control input ω_d is designed as:

$$\omega_d = R^{-1}(-k_e e + \dot{\Omega}_d) \tag{15}$$

where $k_e \in \mathbb{R}^{3\times 3}$ is a positive definite diagonal gain matrix. Substituting (15) into (14) results in:

$$\dot{e} = -k_e e + Rz. \tag{16}$$

Next, the time derivative of (13) is computed, and by using (8) and (10), the following expression is obtained:

$$\begin{aligned} \dot{z} &= \dot{\omega} - \dot{\omega}_d \\ &= F + \Psi\delta + \Psi\beta - \dot{\omega}_d. \end{aligned} \tag{17}$$

Substituting (11) into (17) yields:

$$\dot{z} = N + \Psi\delta + \Psi W^T \sigma \tag{18}$$

where $N(t) \in \mathbb{R}^3$ contains the uncertain terms and is defined as:

$$N \triangleq -\dot{\omega}_d + F + \Psi\varepsilon, \tag{19}$$

which can be upper-bounded by considering (14) and the time derivative of (15), as follows:

$$\| N \| \leq \eta_e \| e \| + \eta_z \| z \| + \mu_n \tag{20}$$

where $\eta_e, \eta_z \in \mathbb{R}^+$ are constants, and $\mu_n \in \mathbb{R}^+$ represents the bound for the remaining terms.

The control law is designed as follows:

$$\delta = \psi^{-1}(-k_z z - R^T e - \delta_g) - \hat{\beta} \tag{21}$$

where $k_z \in \mathbb{R}^{3\times3}$ represents a positive definite, diagonal constant matrix, $\delta_g(t) \in \mathbb{R}^3$ is the component of the control signal used to compensate the uncertain term N, and is defined as:

$$\delta_g = k_g tanh(z) \tag{22}$$

where $k_g \in \mathbb{R}$ is a positive constant, and $tanh(\cdot)\colon \mathbb{R}^3 \to \mathbb{R}^3$ is the hyperbolic tangent function that ensures bounded outputs. Additionally, $\hat{\beta}(t) \in \mathbb{R}^3$ denotes the neural network-based compensation term, defined as:

$$\hat{\beta} = \widehat{W}^T \sigma(X) \tag{23}$$

where X is represented as:

$$X = [\omega_d, \Omega_d, e, z]^T. \tag{24}$$

In Equation (23), $\widehat{W}(t) \in \mathbb{R}^{12\times3}$ is the estimated weight matrix, updated by the following dynamics:

$$\dot{\widehat{W}} = \Gamma_w \Psi \sigma z^T - k_w \|z\| \Gamma_w \widehat{W} \tag{25}$$

where $\Gamma_w \in \mathbb{R}^{12\times12}$ is a positive definite diagonal matrix, $k_w \in \mathbb{R}$ is a positive constant gain, and $\|\cdot\|$ represents the Euclidean norm.

Assumption 3 The ideal neural network weight matrix satisfies the inequality $\| \mathrm{W} \|_{i\infty} \leq \overline{\mathrm{w}}$, where $\overline{\mathrm{w}} \in \mathbb{R}^+$ is a predefined constant and $\|\cdot\|_{i\infty}$ represents the induced infinity norm of a matrix. To guarantee the boundedness of the estimated weight matrix, a projection algorithm can be applied to the right-hand side of (25). As a result, the weight matrix estimation error, defined as $\widetilde{\mathrm{W}}(\mathrm{t}) \triangleq \mathrm{W} - \widehat{\mathrm{W}} \in \mathbb{R}^{12\times3}$, remains bounded, ensuring that $\| \widetilde{\mathrm{W}} \|_{i\infty} \leq \overline{\widetilde{\mathrm{w}}}$, where $\overline{\widetilde{\mathrm{w}}} \in \mathbb{R}^+$ is a known constant.

By substituting (21), (22) and (23), (18) can be rewritten as

$$\dot{z} = N - k_g tanh(z) - k_z z - R^T e + \Psi \widetilde{W} \sigma. \tag{26}$$

For a better understanding, the block diagram of the entire closed-loop control system is depicted in Figure 1.

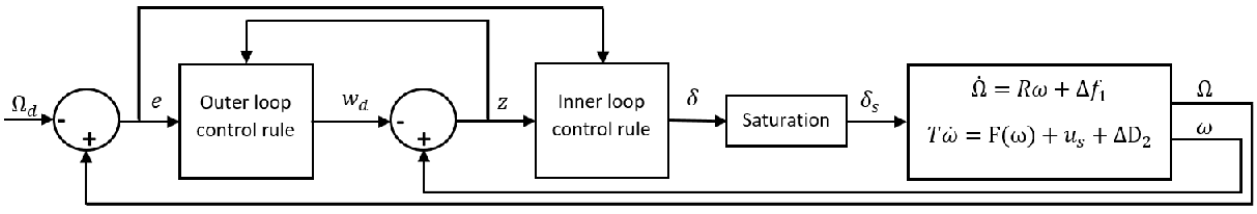

Figure 1. *The block diagram of the closed loop control system*

4. STABILITY ANALYSIS

Theorem 1 The virtual controller described in (15), the control law presented in (21), the auxiliary input defined in (22), and the adaptive estimation rule in (25) collectively ensure that the tracking error e is minimized to a vicinity near zero while maintaining boundedness of all system signals, provided the gains meet the following conditions:

$$\lambda_{\min}(k_z) > \nu + \eta_z + \eta_e^2, \tag{27}$$

$$\lambda_{\min}(k_e) > \frac{1}{4} \tag{28}$$

where $\lambda_{\min}(\cdot)$ denotes the smallest eigenvalue of a matrix, and $\nu > 0$ is an auxiliary positive constant.

Proof. The candidate Lyapunov function $V(t) \in \mathbb{R}$ is selected as:

$$V = \frac{1}{2}e^T e + \frac{1}{2}z^T z + \frac{1}{2}tr\{\widetilde{W}^T \Gamma_w^{-1} \widetilde{W}\}. \tag{29}$$

Using Assumption 3, (29) can be bounded as:

$$\frac{1}{2}\|s\|^2 \leq V \leq \frac{1}{2}\|s\|^2 + \gamma_1 \tag{30}$$

where $s(t) \triangleq [e^T \ \ z^T]^T \in \mathbb{R}^6$ represents the combined error vector. Here, γ_1 is positive constants defined as:

$$\gamma_1 \triangleq \frac{1}{2}\max\{\Gamma_w^{-1}\}\bar{\widetilde{W}}^2. \tag{31}$$

Taking the time derivative of (29) gives:

$$\dot{V} = e^T \dot{e} + z^T \dot{z} + tr\left\{\widetilde{W}^T \Gamma_w^{-1} \dot{\widetilde{W}}\right\}, \tag{32}$$

and substituting (16), (25), and (26) into (32) results in:

$$\begin{aligned} \dot{V} = {} & e^T(-k_e e + Rz) + z^T(N - R^T e - k_g tanh(z) - k_z z + \Psi \widetilde{W}^T \sigma) \\ & -tr\{\widetilde{W}^T \Psi \sigma z^T\} + k_w \|z\| tr\{\widetilde{W}^T \widehat{W}\}. \end{aligned} \tag{33}$$

Using $tr\{ab\} = tr\{ba\}$, (33) simplifies to:

$$\dot{V} = -e^T k_e e + z^T(N - k_g tanh(z)) - z^T k_z z + k_w \|z\| tr\{\widetilde{W}^T \widehat{W}\}. \tag{34}$$

The last term on the right-hand side of Equation (34) can be bounded as follows:

$$\begin{aligned} tr\{\widetilde{W}^T \widehat{W}\} &= tr\{\widetilde{W}^T W\} - tr\{\widetilde{W}^T \widetilde{W}\} \\ &\leq \bar{w} \parallel \widetilde{W} \parallel_{i\infty} - \parallel \widetilde{W} \parallel_{i\infty}^2 \\ &\leq \frac{\bar{w}^2}{4}. \end{aligned} \tag{35}$$

By substituting (35) and considering the property $z^T tanh(z) \geq 0$, Equation (34) can be bounded as

$$\begin{aligned} \dot{V} \leq {} & -e^T k_e e - z^T k_z z \\ & + \left[\parallel z \parallel \parallel N \parallel + k_w \frac{\bar{w}^2}{4} \parallel z \parallel - z^T k_g tanh(z)\right]. \end{aligned} \tag{36}$$

From (20), the following equation can derived:

$$\begin{aligned} \dot{V} \leq {} & -e^T k_e e - z^T k_z z + \parallel z \parallel \eta_e \parallel e \parallel + \eta_z \parallel z \parallel^2 \\ & + \left[\parallel z \parallel \parallel \mu_n \parallel + k_w \frac{\bar{w}^2}{4} \parallel z \parallel - z^T k_g tanh(z)\right]. \end{aligned} \tag{37}$$

The term $\parallel z \parallel \eta_e \parallel e \parallel$ can be upper bounded as:

$$\parallel z \parallel \eta_e \parallel e \parallel \leq \frac{1}{4} \parallel e \parallel^2 + \eta_e^2 \parallel z \parallel^2. \tag{38}$$

The remaining terms in the brackets on the right-hand side of (36) can be bounded as:

$$\parallel z \parallel \zeta \leq \nu \parallel z \parallel^2 + \frac{1}{4\nu}\zeta^2, \tag{39}$$

where $\zeta = \parallel \mu_n \parallel + k_w \frac{\bar{w}^2}{4} - k_g |tanh(z)|$. Setting $\nu \in \mathbb{R}^+$, ζ is guaranteed to be bounded and can be reduced by increasing k_g.

Incorporating (38) and (39) into (37):

$$\begin{aligned}\dot{V} &\leq -(\lambda_{\min}(k_z) - (\nu + \eta_z + \eta_e^2)) \parallel z \parallel^2 \\ &\quad -\left(\lambda_{\min}(k_e) - \frac{1}{4}\right) \parallel e \parallel^2 + \frac{1}{4\nu}\zeta^2 \\ &\leq -\gamma_2 \parallel s \parallel^2 + \gamma_3,\end{aligned} \tag{40}$$

where

$$\gamma_2 \triangleq \min\left\{\lambda_{\min}(k_z) - (\nu + \eta_z + \eta_e^2), \lambda_{\min}(k_e) - \tfrac{1}{4}\right\}, \tag{41}$$

$$\gamma_3 \triangleq \frac{1}{4\nu}\zeta^2, \tag{42}$$

and the conditions in (27) and (28) are satisfied.

Using (30), Equation (40) can be rewritten as:

$$\dot{V} \leq -2\gamma_2 V + 2\gamma_1\gamma_2 + \gamma_3. \tag{43}$$

The solution to (43) is:

$$V \leq \zeta_3 e^{-\zeta_1 t} + \frac{\zeta_2}{\zeta_1}, \tag{44}$$

where $\zeta_1 = 2\gamma_2$, $\zeta_2 = 2\gamma_1\gamma_2 + \gamma_3$, and $\zeta_3 = V|_{t=0} - \frac{\zeta_2}{\zeta_1}$. By meeting the conditions in (27) and (28), and increasing k_g sufficiently, V can be made arbitrarily small.

From (44), it follows that $V \in \mathcal{L}_\infty$, and thus, the error signals e and z are also bounded ($e, z \in \mathcal{L}_\infty$). Using the definitions in (12) and (13), the boundedness of $\Omega(t)$ and $\omega(t)$ can also be guaranteed. As a direct result, the virtual control signal ω_d and the control signal δ remain bounded. By applying standard signal chasing arguments, it can be shown that all remaining signals in the closed-loop system are uniformly bounded, ensuring the ultimate boundedness of the tracking error.

5. NUMERICAL SIMULATIONS

The performance of the proposed control scheme was evaluated through numerical simulations. During these simulations, the parameter values were taken from Table 2. The initial values of the variables were set as $\Omega_0 = [0.1, 0.25, -43.6]^T$ in degrees, $\omega_0 = [0,0,0]^T$ in deg/sec [7], and the initial value of $\widehat{W}$ was set to the zero matrix. The control rules in (15) and (21) were applied with the gains $k_e = \text{diag}\{[6,5,4]\}$, $k_Z = \text{diag}\{[20,20,20]\}$, $k_g = 10$, and the update rule for the weight matrix was implemented with the gains $\Gamma = \text{eye}(12,12) \times 10^{-6}$ and $k_w = 1$, where $\text{eye}(n,n)$ denotes an $n \times n$ identity matrix. The reference values were set to $\Omega_d = [45,30,10]$ in degrees.

The control scheme was tested in both noisy and noise-free scenarios to demonstrate its robustness against noise. In the noisy cases, 20 dB AWGN was added to both the angle and angular rate measurements.

Figures 2 and 3 show the angles and control signals. As observed, the angles successfully track the set points with saturated inputs.

In Figures 4 and 5, the reference signals were chosen as a trajectory. In this scenario, the control signals ensured that the angles tracked the reference signals effectively.

In Figures 6 and 7, the angles and control signals are presented. From the figures, it can be observed that the control scheme maintains its tracking performance with minimal degradation.

Table 2. *Parameter Values [15]*

Parameter	**Value**	**Parameter**	**Value**
C_{p_0}	0	C_{p_β}	-0.1261
C_{p_p}	-0.3167	C_{p_r}	0.1422
C_{m_0}	-0.02338	C_{m_α}	-0.38
C_{m_q}	-3.6	C	0.18994
C_{r_0}	0	C_{r_β}	0.1335
C_{r_p}	-0.0092	C_{r_r}	-0.1892
$C_{p_{\delta_a}}$	0.1031	$C_{p_{\delta_r}}$	0.1260
$C_{m_{\delta_e}}$	-0.5	V_a	17 m/s
ρ	1.2682	β	0.1 rad
α	1.24 rad	m	13.5 kg
I_x	0.8244	I_y	1.135
I_z	1.759	I_{xz}	0.1204
S	0.55 m^2		

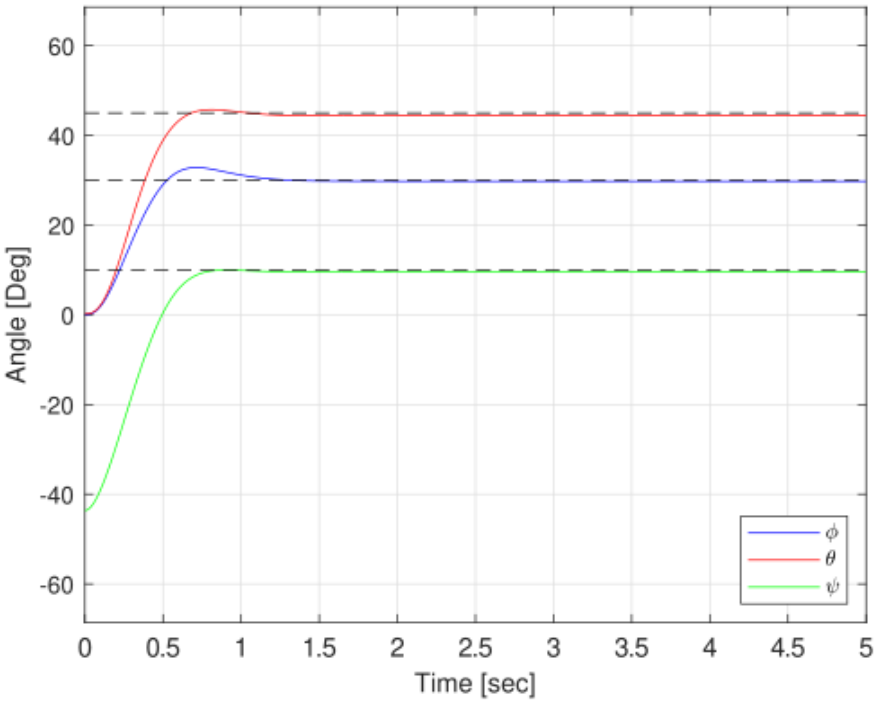

Figure 2. *Angles for noise free case*

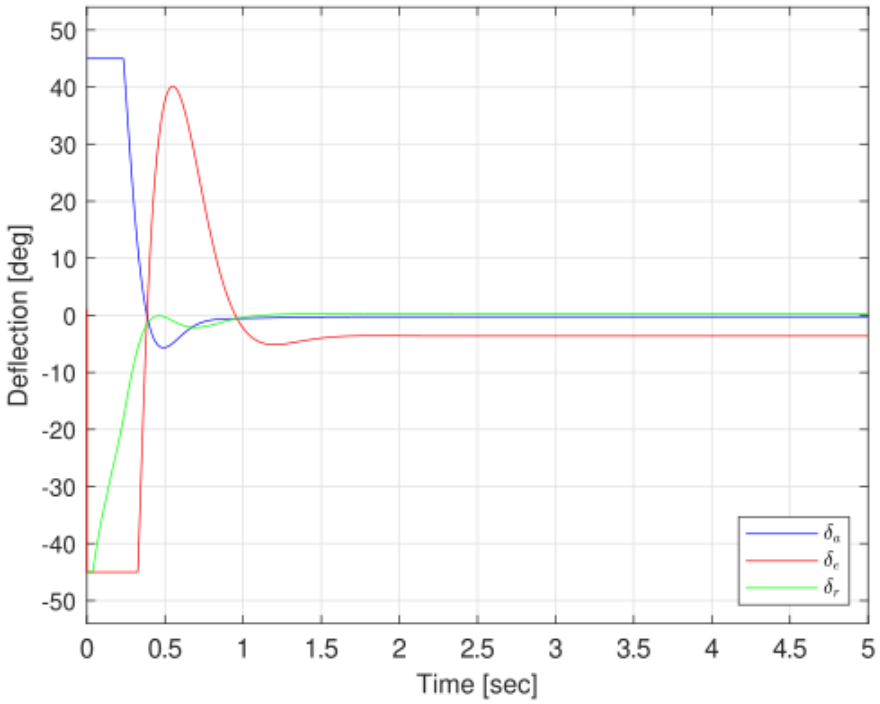

Figure 3. *Control signals for noise free case*

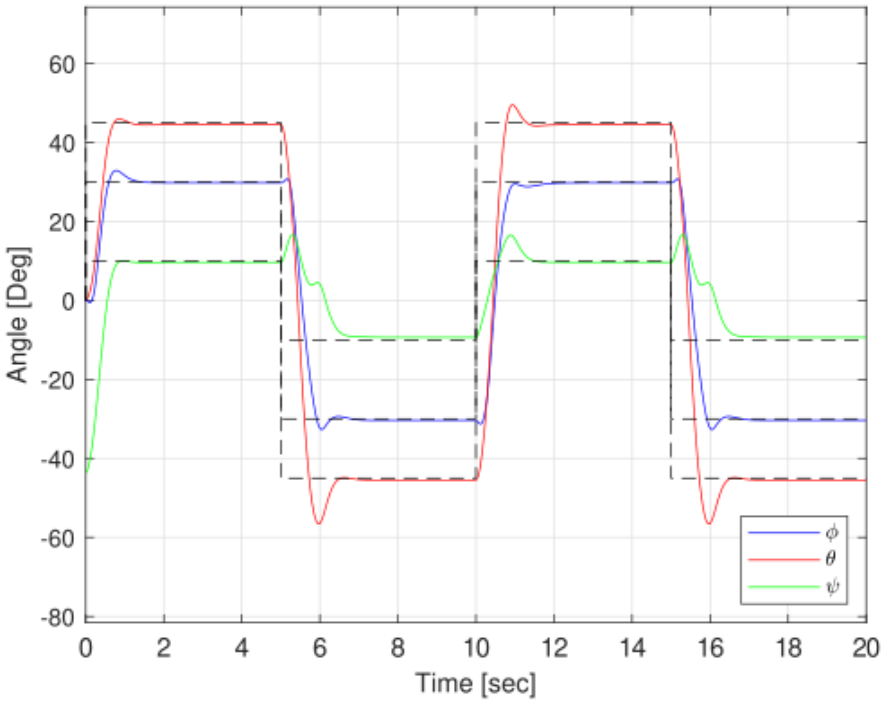

Figure 4. *Angles for trajectory tracking case*

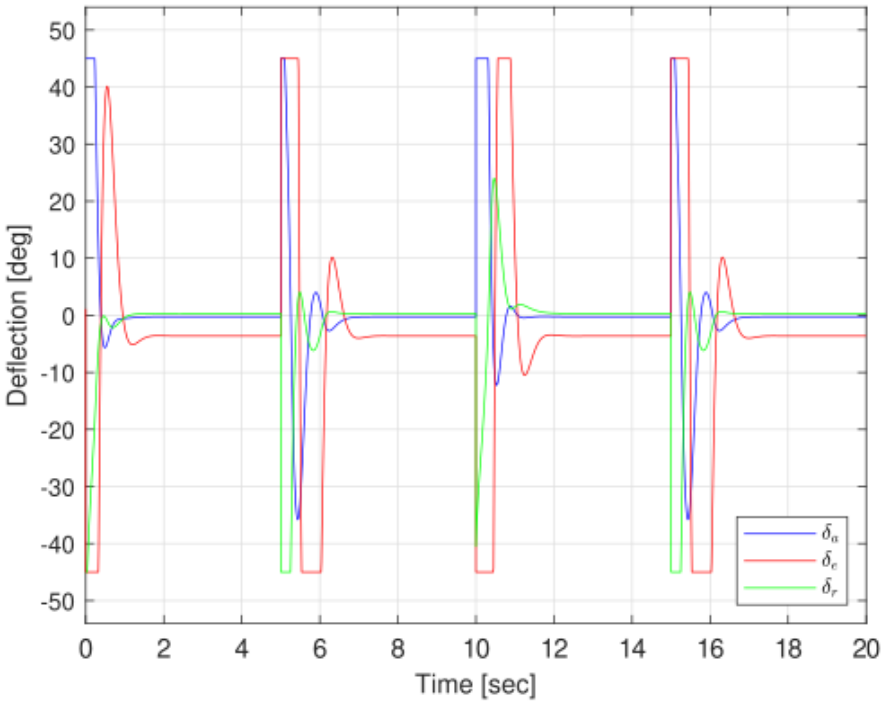

Figure 5. *Control signals for trajectory tracking case*

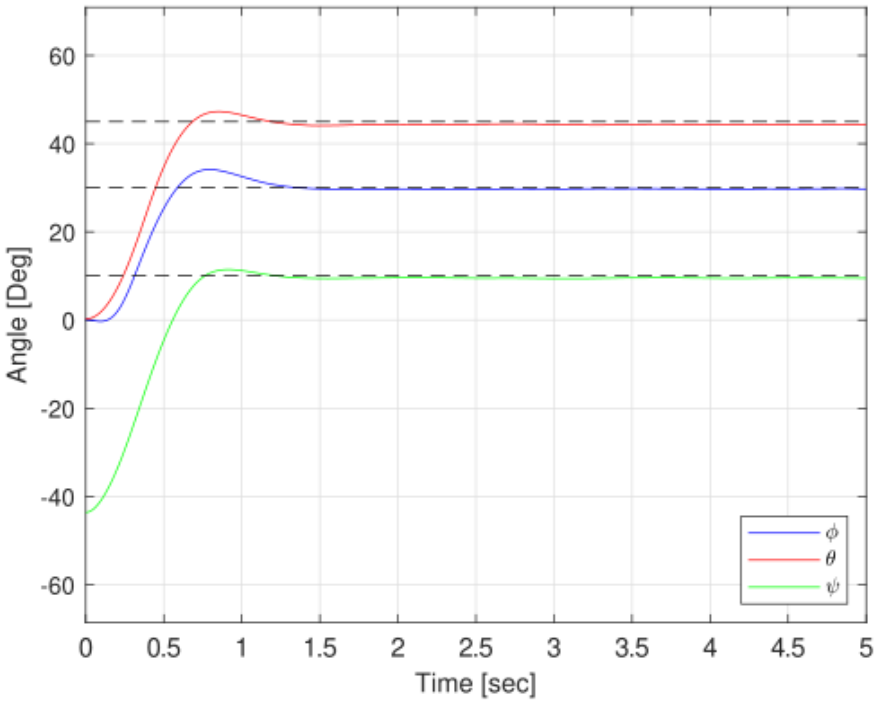

Figure 6. *Angles for noisy case*

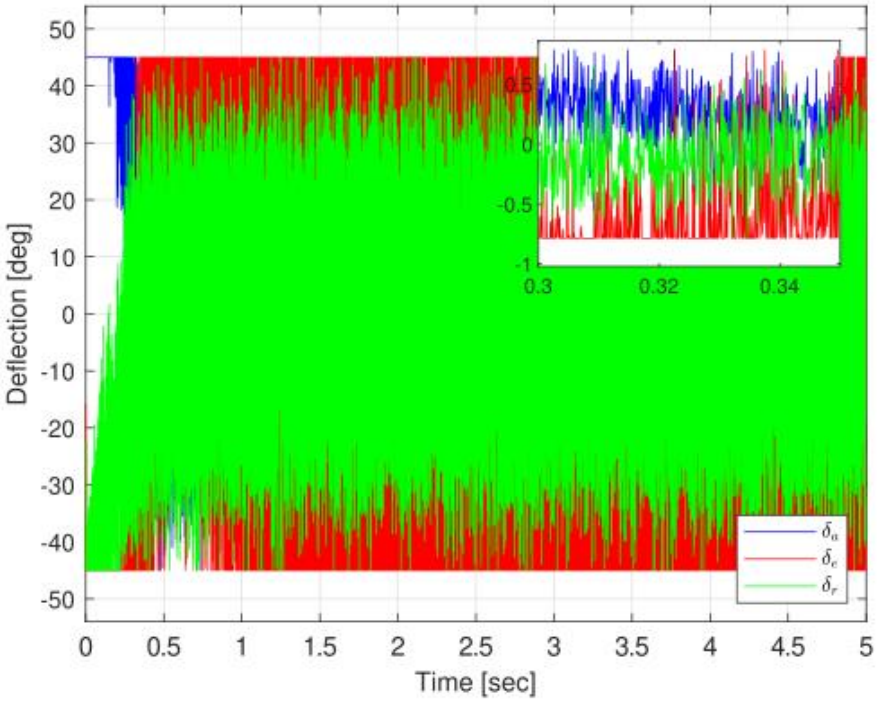

Figure 7. *Control signals for noisy case*

6. COMPARATIVE RESULTS

The performance of the proposed controller was compared with common control techniques, namely PID and sliding mode (SM) control. All the control signals were subjected to the saturation function defined in (9). The comparison was conducted using the error criterion given below:

$$M_c = \sqrt{\int_{t_0}^{t} c^2(\tau) d\tau}, \tag{45}$$

where c represents a signal and t indicates time. Table 3 gives the comparative results, where M_e and M_u correspond to tracking error and control effort performances, respectively. The results clearly indicate that the proposed controller outperformed the compared techniques in terms of both tracking error and control effort.

Table 3. *Comparison results*

Case	**Criteria**	**Proposed**	**PID**	**SM**
Without noise	M_e	0.7078	0.976	0.9376
	M_u	0.7793	1.371	3.042
With noise	M_e	0.8075	1.543	1.505
	M_u	1.492	2.982	3.042

7. CONCLUSIONS

In this study, the attitude control of a fixed-wing UAV under saturated inputs was investigated. The system was analyzed by dividing it into two subsystems, and a high-gain backstepping controller was designed. The control surfaces of the fixed-wing UAV have physical constraints, modeled as input saturation, which negatively affect stability and may even lead to instability. To address this issue, a neural network term was incorporated to mitigate the adverse effects of the residual part of the control. The stability of the control system was analyzed using the Lyapunov method, and the ultimate boundedness of error signals was ensured. The effectiveness of the proposed control system was validated through numerical simulations, demonstrating its capability to maintain stable and reliable performance. Furthermore, it was observed that the control system performed effectively even when noise was added to the state variables.

CONFLICTS OF INTEREST

No conflict of interest was declared by the author.

REFERENCES

[1] Kimathi, S., Lantos, B., "Modelling and attitude control of an agile fixed wing uav based on nonlinear dynamic inversion", Periodica Polytechnica Electrical Engineering and Computer Science, 66(3): 227-235, (2022). DOI: 10.3311/PPee.20287

[2] Melkou, L., Hamerlain, M., Rezoug, A., "Fixed-wing uav attitude and altitude control via adaptive second-order sliding mode", Arabian Journal for Science and Engineering, 43: 6837-6848, (2018). DOI: 10.1007/s13369-017-2881-8

[3] Bao, C., Guo, Y., Luo, L., Su, G., "Design of a fixed-wing uav controller based on adaptive backstepping sliding mode control method", IEEE Access, 9: 157825-157841, (2021). DOI: 10.1109/ACCESS.2021.3130296

[4] Bøhn, E., Coates, E.M., Moe, S., Johansen, T.A., "Deep reinforcement learning attitude control of fixed-wing uavs using proximal policy optimization", IEEE International Conference on Unmanned Aircraft Systems (ICUAS), 523-533, (2019). DOI: 10.1109/ICUAS.2019.8798254

[5] Chen, L., Liu, Z., Dang, Q., Zhao, W., Chen, W., "Robust fixed-time flight controller for a dual-system convertible uav in the cruise mode", Defence Technology, 39: 53-66, (2024). DOI: 10.1016/j.dt.2024.04.009

[6] Poksawat, P., Wang, L., Mohamed, A., "Automatic tuning of attitude control system for fixed-wing unmanned aerial vehicles", IET Control Theory & Applications, 10(17): 2233-2242, (2016). DOI: 10.1049/iet-cta.2016.0236

[7] SaiCharanSagar, A., Vaitheeswaran, S., Shendge, P., "Uncertainity estimation based approach to attitude control of fixed wing UAV", IFAC-PapersOnLine, 49(1): 278-283, (2016). DOI: 10.1049/iet-cta.2016.0236

[8] Ulus, S., Eski, I., "Neural network and fuzzy logic-based hybrid attitude controller designs of a fixed-wing UAV", Neural Computing and Applications, 33(14): 8821-8843, (2021). DOI: 10.1007/s00521-020-05629-5

[9] Zhao, S., Zheng, J., Yi, F., Wang, X., Zuo, Z., "Exponential predefined time trajectory tracking control for fixed-wing uav with input saturation", IEEE Transactions on Aerospace and Electronic Systems, 60(5): 6406-6419, (2024). DOI: 10.1109/TAES.2024.3402656

[10] Yu, Z., Zhang, Y., Jiang, B., Su, C.Y., Fu, J., Jin, Y., Chai, T., "Nussbaum-based finite-time fractional-order backstepping fault-tolerant flight control of fixed-wing uav against input saturation with hardware-in-the-loop validation", Mechanical Systems and Signal Processing, 153: 107406, (2021). DOI: 10.1016/j.ymssp.2020.107406

[11] Li, Z., Chen, X., Xie, M., Zhao, Z., "Adaptive fault-tolerant tracking control of flying-wing unmanned aerial vehicle with system input saturation and state constraints", Transactions of the Institute of Measurement and Control, 44(4): 880-891, (2022). DOI: 10.1177/01423312211027037

[12] Oh, D.D., Lee, D., Kim, H.J., "Safety-critical control under multiple state and input constraints and application to fixed-wing UAV", 62nd IEEE Conference on Decision and Control (CDC), 1748-1755, (2023). DOI: 10.1109/CDC49753.2023.10383422

[13] Wu, J., Wang, H., Li, S., Liu, S., "Distributed adaptive path-following control for distance-based formation of fixed-wing UAVs under input saturation", Aerospace, 10(9): 768, (2023). DOI: 10.3390/aerospace10090768

[14] Gao, W., Selmic, R.R., "Neural network control of a class of nonlinear systems with actuator saturation", IEEE Transactions on Neural Networks, 17(1): 147-156, (2006). DOI: 10.1109/TNN.2005.863416

[15] Beard, R.W., McLain, T.W., "Small unmanned aircraft: Theory and practice", Princeton University Press, UK, (2012). ISBN: 978-0-691-14921-9